RSC Advances

PAPER

View Article Online
View Journal | View Issue

Cite this: RSC Adv., 2015, 5, 96660

Carbonized polyaniline coupled molybdenum disulfide/graphene nanosheets for high performance lithium ion battery anodes†

Sheng Han,‡[a] Yani Ai,‡[a] Yanping Tang,[b] Jianzhong Jiang[a] and Dongqing Wu*[ab]

Received 1st July 2015
Accepted 11th September 2015

DOI: 10.1039/c5ra12750e

www.rsc.org/advances

Two-dimensional molybdenum disulfide/graphene hybrids wrapped in carbonized polyaniline (MCGs) have been constructed by the *in situ* growth of molybdenum trisulfide nanoparticles on polyaniline decorated graphene oxide nanosheets and the following carbonization. When the resulting hybrids were used as anode materials in lithium ion batteries, the carbonized polyaniline can effectively prevent the pulverization of MoS_2 caused by the inner-plane volume expansion. It turns out that MCG-600, the sample thermally treated at 600 °C, manifests a capacity of 785 mA h g^{-1} after 300 cycles at the current density of 200 mA g^{-1} and a capacity of 724 mA h g^{-1} even at a high current density of 1 A g^{-1}.

1. Introduction

Owing to extensive applications in portable electronics, electric vehicles and grid energy storage, lithium ion batteries (LIBs) with high energy density and long cycling life have aroused significant interest from both industry and academia.[1,2] However, the electrochemical performances of current commercial LIBs are still retarded by the intrinsically low theoretical capacities of their graphite anodes (372 mA h g^{-1}) and cannot fulfil the increasing demands for miniature LIBs with higher energy density.[3–5] Therefore, the seeking of unprecedented anode materials with predominant Li storage capacity to replace graphite becomes an urgent task for material scientists.[6–10] Compared with other candidates, the hybrids of carbon and inorganic nanoparticles have manifested overwhelming advantages as the alternatives of graphite anode. In these hybrids, the inorganic species with high theoretical capacities can provide plenty of active sites for lithium storage. On the other hand, the carbon components can ensure the conductivity of the whole electrode and prevent the structural damages caused by the volume expansion of inorganic nanoparticles.[6,11–14]

To build up a hybrid material for LIB anode, molybdenum disulfide (MoS_2), a layered transition-metal dichalcogenide with hexagonal arrays of Mo sandwiched between two S layers, is an appealing choice since it has both high theoretical capacity and favorable interlayer spacing for hosting Li atoms.[15–19] As the carbon component, graphene with excellent conductivity and mechanism stability can effectively facilitate the migration of the electrons and relax the strain from the volume variation of MoS_2.[20–22] Nevertheless, only the inter-plane aggregation of MoS_2 can be inhibited by two-dimensional (2D) graphene sheets. The inner-plane contact and pulverization of MoS_2 on graphene still exist and will sabotage the long term stability of the electrode materials.[23–25]

Herein, we report the facile fabrication of the unprecedented 2D hybrids of carbonized polyaniline (PANI) coupled graphene and MoS_2, named as MCGs, *via* the *in situ* growth of molybdenum trisulfide (MoS_3) nanoparticles on the PANI decorated graphene oxide (GO) nanosheets and the following carbonization of the resulting ternary composites. The resulting hybrids possess well-defined 2D architectures with MoS_2 nanoplates confined in the carbonized PANI. As the coupling linker between graphene and MoS_2, the carbonized PANI can effectively improve the electrochemical performance of MCGs when they serve as the anode materials in LIBs. At a charging rate of 200 mA g^{-1}, MCG-600, the sample thermally treated at 600 °C, can deliver an excellent specific capacity of 785 mA h g^{-1} after 300 charge/discharge cycles. Its capacity can be retained as 724 mA h g^{-1} even at an high current density of 1 A g^{-1}.

2. Experimental

2.1. Materials

Sodium sulfide (Na_2S), sodium molybdate (Na_2MoO_4), and aniline were obtained from Aladdin Reagent Co. Ltd. Sodium dodecyl benzene sulfate (SDBS), ammonium persulfate (APS), hydrochloric acid (HCl, 36 wt%), concentrated sulfuric acid (H_2SO_4, 98%), potassium permanganate ($KMnO_4$), sodium nitrate ($NaNO_3$), and hydrogen peroxide (H_2O_2) were bought

[a]School of Chemical and Environmental Engineering, Shanghai Institute of Technology, Shanghai 201418, China. E-mail: wudongqing@gmail.com
[b]School of Chemistry and Chemical Engineering, Shanghai Jiao Tong University, Shanghai 200240, China

† Electronic supplementary information (ESI) available. See DOI: 10.1039/c5ra12750e

‡ These authors contributed equally to this work.

from Sinopharm Chemical Reagent Co. Ltd. Unless otherwise stated, all the reagents were of analytical grade and used as received. All aqueous solutions were prepared with DI water.

2.2. Preparation of PANI–GO sheets

GO was synthesized from natural graphite flakes by modified Hummers method. To prepare PANI functionalized GO nanosheets (PANI–GO), aniline (300 μL) were first mixed with SDBS (10 mg) in H_2O (50 mL), and the solution was then added to the aqueous dispersion of GO (0.50 mg mL^{-1}, 60 mL). The resulting mixture was ultra-sonicated for 15 min to form a homogeneous suspension. Subsequently, APS (0.7 g) dissolved in HCl (1 M, 50 mL) was added slowly to the suspension, which was vigorously stirred overnight at 0–5 °C. Then the green suspension of PANI–GO was obtained.

2.3. Preparation of MoS_3–PANI–GO hybrids

The obtained green suspension of PANI–GO was heated to 90 °C under stirring and Na_2MoO_4 (300 mg) dissolved in water (30 mL) was added dropwise. The mixture was continuously stirring at 90 °C for 3 h. Then, Na_2S (1.5 g) dissolved in water (30 mL) was added to above mixture quickly, followed by vigorous stirring. After cooling down naturally, the resulting black suspension was centrifuged and washed with water and ethanol for several times to afford MoS_3–PANI–GO.

2.4. Preparation of MCGs

MoS_3–PANI–GO was calcined in a tube furnace at 400, 600 or 800 °C with a heating rate of 5 °C min^{-1} for 3 h under N_2 atmosphere to produce MCGs as the final products.

2.5. Characterization

Scanning electron microscopy (SEM) measurements were performed on a FEI Sirion-200 field emission scanning electron microscope. Transmission electron microscopy (TEM) images were acquired using a Tecnai G2 F20 S-TWIN transmission electron microscope (FEI) operated at 200 kV. The sample was dispersed in ethanol and the suspension was dropped onto a copper grid covered with microgrid film. X-ray diffraction (XRD) analysis was performed on a D/Max-2500 X-ray diffractometer with Cu Kα radiation (λ = 0.1542 nm). FTIR spectra were recorded using Spectrum 100 spectrometer (Perkin Elmer, Inc., USA). Thermogravimetric analysis (TGA) curves were monitored on a Q5000IR apparatus (TA Instruments, USA). X-ray photoelectron spectroscopy (XPS) experiment was carried out on AXIS Ultra DLD system from Kratos with Al Kα radiation as X-ray source for radiation.

2.6. Electrochemical measurements

Electrochemical tests of the hybrids as the anodes in lithium ion batteries (LIBs) were performed under ambient temperature using two-electrode 2032 coin-type cell. Pure lithium foil was used as the counter electrode. A microporous polypropylene membrane was used as the separator. The electrolyte consisting of a solution of 1 M $LiPF_6$ in ethylene carbonate (EC)/dimethyl carbonate (DMC) (1 : 1 by volume) was obtained from Ube Industries Ltd. The working electrodes were prepared by mixing the hybrids (MCG-400, MCG-600, or MCG-800), carbon black (Super-P), and poly(vinyl difluoride) (PVDF) at a weight ratio of 8 : 1 : 1 and pasting the mixture on pure copper foil (99.6%). The electrode was dried at 60 °C for 12 h in a vacuum oven and cut into sheets (Φ = 11 mm). The amount of active materials loaded on the electrode was ~1.5 mg cm^{-2}. The cells were assembled in an argon-filled glove box with the concentrations of moisture and oxygen below 1 ppm. Cyclic voltammogram (CV) test was conducted on a CHI 760 electrochemistry workstation at a scan rate of 0.1 mV s^{-1}. AC impedance spectroscopy was obtained by applying a sine wave with amplitude of 1.5 V over the frequency range from 100 kHz to 0.01 Hz. Galvanostatic charge/discharge measurements were conducted on a battery tester (Land CA2001A) at various current rates in a potential range of 0.01–3.0 V *vs.* Li/Li^+. The capacity was calculated based on the total mass of the active materials.

3. Results and discussion

The fabrication process of the 2D MCG hybrids is illustrated in Scheme 1. At first, GO coated with PANI (PANI–GO) were obtained by the polymerization of aniline in the suspension of GO. The resultant PANI–GO were then mixed with Na_2MoO_4 and Na_2S to allow the *in situ* formation of MoS_3–PANI–GO with MoS_3 nanoparticles loading on the surface of the nanosheets. During this process, PANI can help the absorption of the inorganic precursors and provide confined spaces for the growth of MoS_3 nanoparticles in case of the unwanted aggregations.[26] To verify the role of PANI, MoS_3–GO was also prepared in this work by the direct growth of MoS_3 NPs on the surface of GO. Subsequently, the resulting MoS_3–PANI–GO nanosheets were thermally treated at 400, 600 or 800 °C to generate MCGs as the final products. According to the pyrolysis temperatures, the samples are denoted as MCG-400, MCG-600 and MCG-800, respectively. In the thermal treatment, MoS_3 is converted to MoS_2 and GO can be thermally reduced. At the same time, nitrogen (N) doped carbon can be produced by the pyrolysis of PANI,[27] which can serve as the protective shell for MoS_2 and enhance the conductivity of the hybrids simultaneously.

The morphologies and microstructures of MoS_3–PANI–GO and MCGs were first investigated by field-emission scanning electron microscopy (FE-SEM) and transmission electron microscopy (TEM). The SEM images (Fig. 1 and S1†) indicate that MoS_3–PANI–GO has typical 2D sheet-like morphology with the fully decoration of PANI particles (5–10 nm) on the surface. The presence of MoS_3 NPs with the size of ~2 nm can be observed in the TEM image of MoS_3–PANI–GO (Fig. 1b).

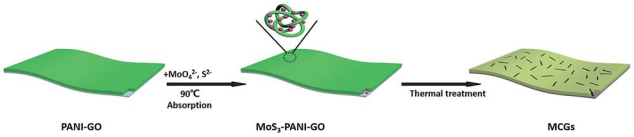

Scheme 1 Schematic illustration for the fabrication process of MCGs.

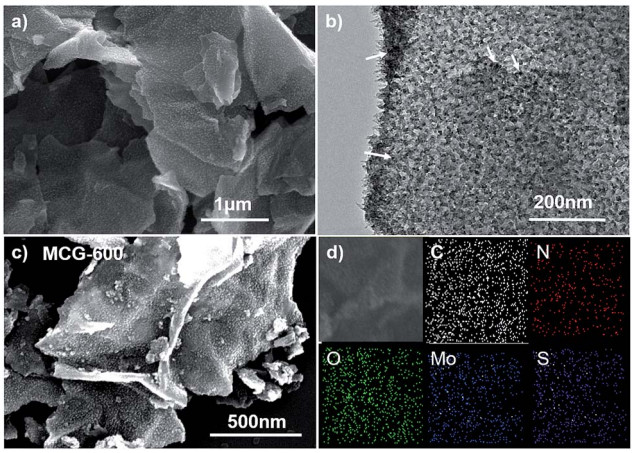

Fig. 1 (a and b) SEM and (b) TEM images of MoS_3–PANI–GO; (c) SEM image of MCG-600; (d) EDX with elemental mapping images of MCG-600.

Without the confining effect of PANI, MoS_3 NPs (having the diameters of ~100 nm) manifest strong aggregation on the surface of MoS_3–GO (Fig. S1†). As indicated by their SEM and TEM images, MCGs still keep the 2D architectures of their precursors after the thermal treatment (Fig. 1c, 2 and S2†). EDX and elemental mapping images further disclose that C, N, O, Mo and S elements are homogeneously distributed in MCG-600 (Fig. 1d). With the increase of the thermal treatment temperature, the edges of the MCG hybrids become smoother and the contrasts of the bright and dark areas are gradually weaker (Fig. 2), implying the reducing amount of the carbonized PANI components. These results are in accordance with the thermogravimetric analysis (TGA) results of the MCG hybrids (Fig. S3†).

To evaluate the crystalline degree of the components in the hybrids, the X-ray diffraction (XRD) patterns of MoS_3–PANI–GO, MCG-400, MCG-600 and MCG-800 were compared in Fig. 3. For MoS_3–PANI–GO, two wide peaks at 14.5° and 42° are contribute to amorphous MoS_3,[28,29] and the peaks at 20°, 26.2° and 28° are from the crystallized PANI and graphene.[30] In contrast, almost

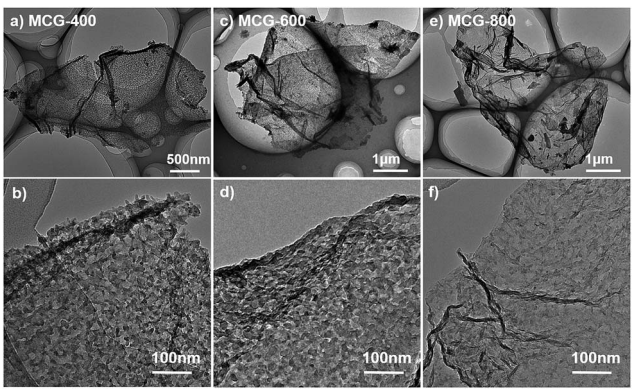

Fig. 2 TEM images of the MCGs: (a and b) MCG-400, (c and d) MCG-600 and (e and f) MCG-800.

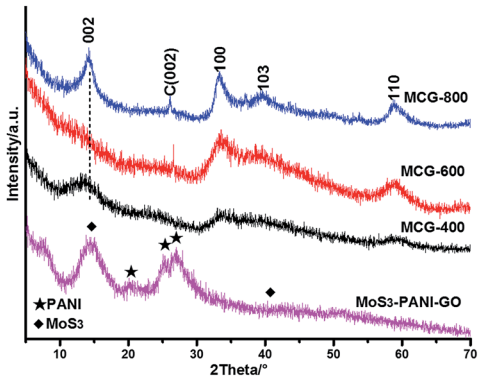

Fig. 3 XRD patterns of MoS_3–PANI–GO, MCG-400, MCG-600 and MCG-800.

all of the diffractions in the XRD patterns of the MCGs can be indexed as the hexagonal phase MoS_2 (JCPDS no. 37-1492),[31] which confirms the conversion of MoS_3 to MoS_2 during the thermal treatment. Moreover, the intensities of the diffraction peaks from MoS_2 gradually increase with the elevated thermal treatment temperature, indicative of the improved crystalline degree of the MoS_2 components in the MCG hybrids.[32]

X-ray photoelectron spectroscopy (XPS) was further applied to analyze the chemical states of the elements in MoS_3–PANI–GO and MCGs. As shown in Fig. 4a, C, N, O, Mo and S elements can be found in MoS_3–PANI–GO and the calculated atomic ratio of Mo to S element is around 1 to 3, which further imply the existence of MoS_3 in the composite.[33–35] Further, as indicated by the XPS spectra of MCGs (Fig. S4†), all the hybrids contain C, N, O, Mo and S elements and the calculated atomic ratio of Mo to S element is 1 to 2, approaching the theoretical value of MoS_2. Additionally the atomic contents of N in MCG-400, MCG-600 and MCG-800 are 13.35, 13.13, and 9.9%, respectively. Further, high-resolution N 1s spectra of MCG-600 discloses that *N* configurations with 22% graphite *N* (401.5 eV), 28% pyridic *N* (398.5 eV) and 50% pyrrolic *N* (400.2 eV) are presented in the hybrid (Fig. 4b).[36]

The combination of MoS_2 and N-doped carbon from PANI in 2D graphene nanosheets makes the MCG hybrids attractive anode materials in LIBs. First, the electrochemical behavior of MCG-600 was investigated by cyclic voltammogram (CV) in the voltage range of 0.001–3 V at a scanning rate of 0.001 mV s^{-1}. As shown in Fig. S5,† in the first cathodic scan, the peak at 1.67 V

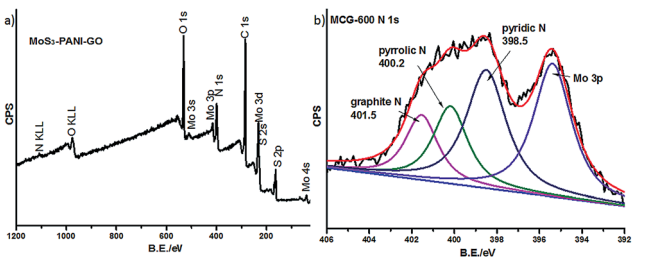

Fig. 4 (a) XPS survey spectra of MoS_3–PANI–GO; (b) XPS spectra of N 1s for MCG-600.

can be assigned to the intercalation of lithium into MoS_2 to form Li_xMoS_2,[31] while the peak at 0.4 V is attributed to the reduction of Li_xMoS_2 to Mo and Li_2S.[6,37] In the anodic scans, the peaks around 1.45 and 2.2 V can be associated with the conversions of Mo to MoS_2 along with Li_2S to polysulfide.[31,37] In the subsequent cathodic scans, two reductive peaks appearing at 1.9 and 1.21 V should be derived from $2Li^+ + S + 2e^- \rightarrow Li_2S$ and $MoS_2 + xLi^+ + xe^- \rightarrow Li_xMoS_2$, respectively.[6,37] The electrochemical performances of MCGs were then evaluated by galvanostatic charge–discharge cycling at a current density of 100 mA g^{-1} in the voltage window of 0.01 to 3 V (Fig. 5a). The initial discharge and charge capacities of MCG-600 are 1554 and 1279 mA h g^{-1}, respectively, corresponding to a coulombic efficiency (CE) of 82.3%. The irreversible loss in capacity is mainly due to electrolyte decomposition and the formation of a gel-like polymeric layer on the surface of electrode (solid electrolyte interface, SEI).[37] The cycling performances of MCGs at a relatively high current density of 200 mA g^{-1} are then compared in Fig. 5b. Among the samples, MCG-400 only delivers a capacity of 315 mA h g^{-1} after 300 charge/discharge cycles. For the electrode based on MCG-600, its specific capacity can be kept as 785 mA h g^{-1} even after 300 cycles. In contrast, the capacity of MCG-800 is retained as 680 mA h g^{-1} under the same conditions.

Beside the excellent cycling stability, MCG-600 also exhibits the remarkable rate performance (Fig. 5c). Its specific capacities at 100, 200, 500, 1000, 2000, to 5000 mA g^{-1} are ~1100, 939, 832, 724, 618 and 456 mA h g^{-1}, respectively. And a reversible capacity of around 1100 mA h g^{-1} is restored when the current density is reset to 100 mA g^{-1}. In contrast, MCG-800 and MCG-400 only have inferior capacities to MCG-600 at various current densities in the range of 100–5000 mA g^{-1}.

The superior lithium storage performance of MCG-600 could be attributed to the synergistic effect of N-doped carbon from PANI, MoS_2, and graphene. The N-doped carbon wrapping around MoS_2 nanoplates can be utilized as the protective shell to buffer the volume expansion of MoS_2 nanoplates during the charge/discharge process. On the other hand, the existence of N-doped carbon can also effectively improve the conductivity of the electrode. The MoS_2 nanoplates confined in N-doped carbon from PANI can favorably provide highly accessible Li storage sites with both minimized insertion distance and interfacial storage.[6] Moreover, the N atoms in the carbon framework of MCGs can both improve the electrolyte wettability of the electrode and provide extra active sites for the storage of lithium. Among the three samples, MCG-600 holds the balance between the content of N-doped carbon and the crystalline degree of MoS_2 nanoplates and carbon frameworks, which endows it the outstanding electrochemical performance as the LIB anode. This can be confirmed by the electrochemical impedance spectra (EIS) of the three electrodes after 300 cycles. As shown in Fig. 5d, the diameter of semi-circle at high frequencies is remarkably reduced in the plot of MCG-600, compared with those of MCG-400 and MCG-800, indicating the greatly decreased charge-transfer resistance at the electrode/electrolyte interface due to the N-enriched carbon and graphene substrate in MCG-600.

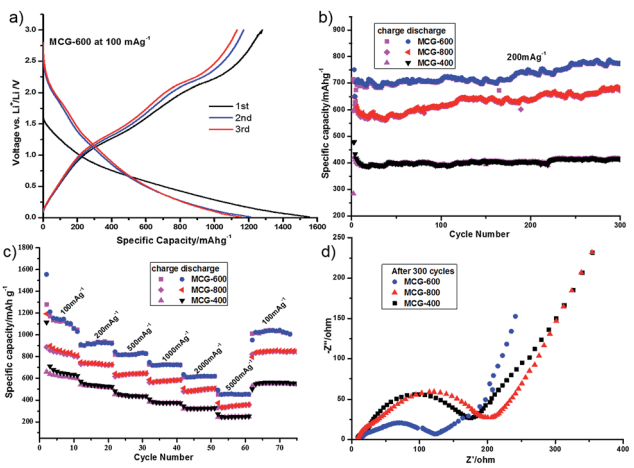

Fig. 5 (a) Charging–discharging curves at 100 mA g^{-1} of the first 3 cycles for MCG-600. (b) Cycling performance of MCGs at 1000 mA g^{-1}. (c) Rate performances of MCGs at different current densities. (d) Nyquist plots of MCGs electrodes.

4. Conclusions

In this work, a facile strategy towards carbonized PANI coupled MoS_2/graphene nanosheets was developed. Among the three MCG hybrids, the one thermally treated at 600 °C manifests the best electrochemical performance as the anode in LIBs, which should be owing to the efficient combination of N-doped carbon, MoS_2 and graphene. The present synthetic strategy can be further extended to the construction various 2D hybrids with promising applications in catalysis, sensors, and other secondary batteries.

Acknowledgements

This work was financially supported by 973 program of China, (2014CB239701 and 2013CB328804), Natural Science Foundation of China (61235007, 61171037, and 21372155), Program of Professor of Special Appointment (Eastern Scholar), Shanghai Leading Academic Discipline Project (Project number 11SG54), ShuGuang Project, Shanghai Talent Development Funding (201335). We also thank the Instrumental Analysis Center of Shanghai Jiao Tong University for providing the relating measurements in this work.

Notes and references

1 A. Yoshino, *Angew. Chem., Int. Ed.*, 2012, **51**, 5798.
2 P. G. Bruce, S. A. Freunberger, L. J. Hardwick and J.-M. Tarascon, *Nat. Mater.*, 2012, **11**, 19.
3 K. S. Novoselov, A. K. Geim, S. Morozov, D. Jiang, Y. Zhang, S. A. Dubonos, I. Grigorieva and A. Firsov, *Science*, 2004, **306**, 666.
4 A. K. Geim, *Science*, 2009, **324**, 1530.
5 A. K. Geim and K. S. Novoselov, *Nat. Mater.*, 2007, **6**, 183.

6 C. Zhu, X. Mu, P. A. van Aken, Y. Yu and J. Maier, *Angew. Chem., Int. Ed.*, 2014, **53**, 2152.
7 Y. Hou, J. Li, Z. Wen, S. Cui, C. Yuan and J. Chen, *Nano Energy*, 2014, **8**, 157.
8 H. Wang, H. Feng and J. Li, *Small*, 2014, **10**, 2165.
9 K. Chang, Z. Wang, G. Huang, H. Li, W. Chen and J. Y. Lee, *J. Power Sources*, 2012, **201**, 259.
10 P. G. Bruce, B. Scrosati and J. M. Tarascon, *Angew. Chem., Int. Ed.*, 2008, **47**, 2930.
11 L. Mai, X. Xu, C. Han, Y. Luo, L. Xu, Y. A. Wu and Y. Zhao, *Nano Lett.*, 2011, **11**, 4992.
12 H. S. Li, X. Y. Wang, B. Ding, G. Pang, P. Nie, L. F. Shen and X. G. Zhang, *ChemElectroChem*, 2014, **1**, 1118.
13 L. Zhang and X. W. D. Lou, *Chem.–Eur. J.*, 2014, **20**, 5219.
14 X. Y. Yu, H. Hu, Y. Wang, H. Chen and X. W. D. Lou, *Angew. Chem., Int. Ed.*, 2015, **54**, 5331.
15 H. Ramakrishna Matte, A. Gomathi, A. K. Manna, D. J. Late, R. Datta, S. K. Pati and C. Rao, *Angew. Chem., Int. Ed.*, 2010, **122**, 4153.
16 S. Wang, X. Jiang, H. Zheng, H. Wu, S.-J. Kim and C. Feng, *Nanosci. Nanotechnol. Lett.*, 2012, **4**, 378.
17 K. Chang and W. Chen, *ACS Nano*, 2011, **5**, 4720.
18 L. Yang, S. Wang, J. Mao, J. Deng, Q. Gao, Y. Tang and O. G. Schmidt, *Adv. Mater.*, 2013, **25**, 1180.
19 H. Liu, D. Su, R. Zhou, B. Sun, G. Wang and S. Z. Qiao, *Adv. Eng. Mater.*, 2012, **2**, 970.
20 S. Ding, J. S. Chen and X. W. D. Lou, *Chem.–Eur. J.*, 2011, **17**, 13142.
21 X. Zhou, L.-J. Wan and Y.-G. Guo, *Nanoscale*, 2012, **4**, 5868.
22 H. Jiang, D. Ren, H. Wang, Y. Hu, S. Guo, H. Yuan, P. Hu, L. Zhang and C. Li, *Adv. Mater.*, 2015, **27**, 3687.
23 K. Chang and W. Chen, *Chem. Commun.*, 2011, **47**, 4252.
24 S. K. Das, R. Mallavajula, N. Jayaprakash and L. A. Archer, *J. Mater. Chem.*, 2012, **22**, 12988.
25 J. Xiao, D. Choi, L. Cosimbescu, P. Koech, J. Liu and J. P. Lemmon, *Chem. Mater.*, 2010, **22**, 4522.
26 S. Li, D. Wu, C. Cheng, J. Wang, F. Zhang, Y. Su and X. Feng, *Angew. Chem., Int. Ed.*, 2013, **125**, 12327.
27 H. Peng, Z. Mo, S. Liao, H. Liang, L. Yang, F. Luo, H. Song, Y. Zhong and B. Zhang, *Sci. Rep.*, 2013, **3**, 1765.
28 P. Afanasiev and I. Bezverkhy, *Chem. Mater.*, 2002, **14**, 2826.
29 X. C. Song, Y. Zhao, Y. F. Zheng and E. Yang, *Adv. Eng. Mater.*, 2007, **9**, 96.
30 Q. Gao, S. Wang, Y. Tang and C. Giordano, *Chem. Commun.*, 2012, **48**, 260.
31 Y. Tang, D. Wu, Y. Mai, H. Pan, J. Cao, C. Yang, F. Zhang and X. Feng, *Nanoscale*, 2014, **6**, 14679.
32 S. Wang, Q. Gao, Y. Zhang, J. Gao, X. Sun and Y. Tang, *Chem.–Eur. J.*, 2011, **17**, 1465–1472.
33 T. Weber, J. Muijsers, J. van Wolput, C. Verhagen and J. Niemantsverdriet, *J. Phys. Chem.*, 1996, **100**, 14144.
34 J. Iranmahboob, S. D. Gardner, H. Toghiani and D. O. Hill, *J. Colloid Interface Sci.*, 2004, **270**, 123.
35 Y. H. Chang, C. T. Lin, T. Y. Chen, C. L. Hsu, Y. H. Lee, W. Zhang, K. H. Wei and L. J. Li, *Adv. Mater.*, 2013, **25**, 756.
36 Y.-H. Chang, R. D. Nikam, C.-T. Lin, J.-K. Huang, C.-C. Tseng, C.-L. Hsu, C.-C. Cheng, C.-Y. Su, L.-J. Li and D. H. Chua, *ACS Appl. Mater. Interfaces*, 2014, **6**, 17679.
37 S. Han, Y. Zhao, Y. Tang, F. Tan, Y. Huang, X. Feng and D. Wu, *Carbon*, 2015, **81**, 203.

